

Porous organic polymers based on cobalt corroles for carbon monoxide binding

Stéphane Brandès, Valentin Quesneau, Osian Fonquernie, Nicolas Desbois, Virginie Blondeau-Patissier, Claude P Gros

▶ **To cite this version:**

Stéphane Brandès, Valentin Quesneau, Osian Fonquernie, Nicolas Desbois, Virginie Blondeau-Patissier, et al.. Porous organic polymers based on cobalt corroles for carbon monoxide binding. Dalton Transactions, 2019, 48 (31), pp.11651-11662. 10.1039/c9dt01599j . hal-03481058

HAL Id: hal-03481058
https://hal.science/hal-03481058

Submitted on 15 Dec 2021

HAL is a multi-disciplinary open access archive for the deposit and dissemination of scientific research documents, whether they are published or not. The documents may come from teaching and research institutions in France or abroad, or from public or private research centers.

L'archive ouverte pluridisciplinaire **HAL**, est destinée au dépôt et à la diffusion de documents scientifiques de niveau recherche, publiés ou non, émanant des établissements d'enseignement et de recherche français ou étrangers, des laboratoires publics ou privés.

Porous Organic Polymers based on Cobalt Corroles for Carbon Monoxide Binding

Stéphane Brandès,[*a] Valentin Quesneau,[a] Osian Fonquernie,[a] Nicolas Desbois,[a] Virginie Blondeau-Patissier,[b] and Claude P. Gros[a]

[a] *Université Bourgogne Franche-Comté, ICMUB (UMR CNRS 6302), 9 Avenue Alain Savary, BP 47870, 21078 Dijon, Cedex, France. E-mail: sbrandes@u-bourgogne.fr*

[b] *Department Time-Frequency, Université Bourgogne Franche-Comté, Institut FEMTO-ST (UMR CNRS 6174), 26 Chemin de l'épitaphe, 25030 Besançon Cedex, France*

Keywords: Porous organic polymers, cobalt corroles, carbon monoxide, microporous materials

Abstract

Porous organic polymers (POPs), known for their high surface area and porosity, were prepared starting from tetraphenyl tetrahedral-shape building blocks and corrole macrocyclic linkers either as free base or cobalt complexes. This synthetic method allowed us to construct new porous frameworks with high carbon monoxide adsorption properties. Two synthetic strategies were developed for incorporating cobalt corroles into the porous matrix. The first method is based on the copper-free Sonogashira cross-coupling reaction between a free base diodo-corrole with a tetrahedral shape derivative followed by cobalt complexation of the resulting material, leading to **POP-CorCo-1**. The second strategy consists to prepare **POP-CorCo-2** by directly using in the coupling reaction the metalated cobalt corrole temporarily protected by two ammine ligands in axial position. The design principles as well as the relationship between the structure and the selective CO adsorption performance are presented. The adsorption capacities and selectivities for CO were calculated from a multisite Langmuir isotherm model and using IAST theory. Spectroscopic studies (NMR, FTIR, UV-visible), kinetic sorption measurements and microscopic analyses made it possible to provide a fairly complete description of the structure of the POPs, their porosity and the nature of solid-gas interactions. The POPs prepared by both methods show a high permanent porosity and outstanding CO sorption properties with a high selectivity over N_2, O_2 and CO_2, up to 15700, 4000 and 1800, respectively. The two **POP-CorCo** offer therefore confined molecular spaces for ascertaining a high accessibility of the metallocorrole active sites for gas binding on the cobalt atom, thus featuring high potential for applications in selective capture or sensing of CO *versus* N_2, O_2 and CO_2.

Introduction

Carbon monoxide (CO), known as the silent killer, is an invisible and odourless gas created by incomplete combustion of fossil fuels. CO is responsible for ~30,000 poisonings in Europe and in the US, giving rise to ~400 and up to 2000 deaths per year in these two areas, respectively.[1,2] Accidental CO intoxications concern each year about 1000 homes and more than 3000 people in France and cause more than 60 deaths *per* year. According to the French public health organization, the number of reported CO intoxication during the 2016-2017 heating season increased by 24% over the previous years. Carbon monoxide poisoning is the most common form of fatal poisoning in France and in the US.

CO is a well-known poisonous pollutant which combines with haemoglobin (Hb) to form "carboxyhemoglobin" (HbCO), and the HbCO adduct is more than 200 times stable than HbO_2 dioxygen adduct.[3] The affinity of four- and five-coordinate iron(II) porphyrins in Hb towards CO is well-documented for the enzymes cytochrome P450,[4] hemoglobin,[5] and myoglobin.[6] This high affinity of hemoglobin and myoglobin for CO *versus* O_2 is the main cause of carbon monoxide poisoning in humans.[7] Symptoms become severe at a concentration of CO above 500 ppm. The World Health Organization has established a reasonable threshold of ~10 ppm for an exposure of 8 hours.[8] Hence, the need to detect and accurately measure this gas is very important in various areas, including health and energy. Although CO detectors are already available, it remains a societal need for marketing small and inexpensive sensing devices with both high sensitivity and selectivity to prevent CO poisoning in indoor and industrial environments. An industrial application of CO sensors is the development of online monitoring and diagnostics systems for durable fuel cell system operations.[9,10] Therefore, there is clearly a high potential for improvements the efficiency and selectivity of CO sensors

technology in a real (air) or synthetic (H_2 used in proton exchange membranes for fuel cell applications) atmosphere in *sub*-ppm concentrations.

Most of the commercial CO detectors are based on electrochemical cells[11] or semiconducting metal oxides such as SnO_2 and ZnO,[12-14] However these sensors operate at high temperatures and suffer from relatively poor selectivity, due to gaseous interference from other common pollutants including humidity, NOx, NH_3, SO_2, and H_2S.[15-19]

Hence, some progress is still to be gained for the development of efficient CO sensors. One crucial point consists to find molecules or metal complexes able to selectively bind CO with a high affinity. Recently, chromogenic and fluorogenic CO sensors were reported based on metallic complexes with Ru(II), Rh(II) and Os(II) complexes for colorimetric detection of CO down to ppm levels.[20-24] Ideal optical sensors should not only display both selectivity and sensitivity towards the desired analyte, but also be air- and photo-stable. In this context, binuclear rhodium and mononuclear ruthenium complexes were notable for the unambiguous colour and emission changes in the presence of increasing concentrations of CO. Once immobilized on silica gel, the reaction with CO in air takes place in few minutes and a limit of detection was estimated to 1 ppm.[21] However, the reversibility of these systems was not clearly established and no specific detection device was built for CO sensing in real conditions.

Fabrication of hierarchical materials containing hollow or 3D structures is a powerful approach to obtain single-phase materials with functionalities hanging in the pores or located in the framework.[25-27] Porous materials like metal–organic frameworks (MOFs) containing unsaturated metal sites, which are capable of binding to CO molecules, have recently been identified as the most promising class of adsorbents for CO adsorption, separation and detection.[28-31] In general, it is far greater for CO uptake and selectivity to include highly specific and energetic unsaturated metal sites than enhancing the surface area and electric

field gradient, which only result in physisorption interactions on the surface.[32] Therefore, when CO adsorption is dominated by gas-metal interactions, higher selectivity over other gases can be expected. However, these materials generally suffer from a lack of selectivity over O_2 since the unsaturated metallic clusters generally bind CO and O_2. To the best of our knowledge, no porous organic or inorganic polymers have been described in the literature with high selective CO adsorption properties. It is thus necessary to construct porous materials functionalized by active complexes for CO binding in view to provide the material with selective gas capture and sensing.

Cobalt metallocorroles are a class of molecules belonging to the porphyrinoid family that are able to coordinate CO at the cobalt(III) center with no interference with O_2 and N_2 since no coordination of these gas occurs on the metal.[33-35] Therefore, the introduction of such molecular complexes in a porous solid should confer the same properties to the material. In our recent investigations, cobalt corroles based materials have demonstrated high affinity for CO binding and promising results have been obtained by our group and others[33-35] for the elaboration of design CO sensors associated with a sensible technology transduction process.[36] However, more convincing results have to be obtained in virtue of the relative instability of cobalt corrole in its tetracoordinated active state, that means without axial donor ligands. We have very recently addressed this problem and shown that cobalt corroles can be stabilized and easily isolated in air atmosphere without any degradation when the coordination sphere of the metal center is fulfilled with one or two labile axial ligands chosen between DMSO or ammonia, these latter acting as “protecting groups”.[37] In addition, the binding properties of CO on metallocorroles is still poorly understood but is relevant with respect to the ubiquity of this gas in polluted air. Permanent porosity and stability are prerequisites for various applications of a material for gas separation or sensing. Therefore, the main goal that we pursue address the incorporation of such active complexes in a porous

framework for a selective CO adsorption or sensing while maintaining the permanent porosity.

Porous solids such as MOFs have been investigated for the formation of various hierarchical structures but their stability is often far to be optimal for subsequent applications due to the lability of most of the metal-donor atom bonding. As an alternative to this main drawback, Porous Organic Polymers (POPs) including Covalent Organic Frameworks (COFs) were emerging in the last ten years as a new class of porous materials that are constructed by linking organic building units together *via* covalent bonds.[38-40] Compared to MOFs constructed with organic ligands connected through coordination bonds, POPs show superior thermal and chemical stability under solvo- or hydrothermal conditions owing to their covalent network. Hence, over the past decade, considerable efforts have been devoted to the construction of new structures with various linkages like *e.g*. aryle groups functionalized by halides, amine or aldehyde. POPs are also promising sorbent materials due to their high surface areas, their permanent porosity and tailorability in the nanometer-scale which make them ideal materials for gas adsorption and separation,[41-44] catalysis,[43,45,46] and energy storage.[47] In particular, the confined space in POP and the control of their pore environment make them attractive materials for sensing applications. However, in view of their great structural variety, surprisingly only few examples have been reported to date in this field, mainly for the detection of explosive aromatic compounds[48,49] or toxic metal ions.[38,50]

For specific applications such as catalysis and gas separation, porphyrins constitute one of the most interesting building block for POP and COF elaboration.[51-54] However, the research with other porphyrinoid derivatives never focused to date on the design of porous structures functionalized by metallocorrole complexes. Actually, it still remains an outstanding synthetic challenge to fine-tune and control the growth of polymeric 3D networks incorporating corrole derivatives.

In order to avoid the stacking of metallocorroles in the polymer and to give the material a high affinity and selectivity for CO adsorption, one possible pathway is to prepare 3D architectures with a diamond topology using tetrahedral-shape building blocks as nodes of the framework.[55] In addition, extended tetrahedral symmetry is advantageous during porosity formation in material synthesis by impeding close packed arrangement of the corrole complexes.[43,47,56-58] This will provide an appealing opportunity to develop robust porous solids with high loadings of isolated sites. Using this strategy, we now wish to report the design and full characterization of new 3D POP materials incorporating (tetraphenyl)methane building blocks and cobalt corrole complexes that are able to selectively bind carbon monoxide in the presence of other gases such as O_2, N_2 and CO_2.

Experimental

Chemicals and materials

Tetrakis(4-ethynylphenylmethane) **2**,[55] corrole **1**[59] and metallocorrole **3**[37] were prepared according to previously published procedures. Additional information is given in the Supporting Information.

Synthesis of POP-Cor. Under inert atmosphere free base diiodocorrole **1** (100 mg, 0.128 mmol, 1 eq) and bis(triphenylphosphine)palladium(II) dichloride (7.2 mg, 0.010 mmol, 0.04 eq *per* alkyne function) were heated at 70 °C in dry tetrahydrofuran (40 mL) and triethylamine (15 mL). A solution of tetra-alkyne **1** (26.7 mg, 0.064 mmol) in dry tetrahydrofuran (30 mL) was added dropwise during 2 h. The solution was stirred for 24 h at 70 °C and cooling down at room temperature, giving a black precipitate which was filtered, washed with tetrahydrofuran and methanol and dried under vacuum. Yield is 82% (78 mg). The characterization data are given in the SI.

Synthesis of POP-CorCo-1. POP-Cor (100 mg) was suspended in degassed DMSO (12 mL) and a solution of cobalt acetate in DMSO (67 mg in 8 mL) was added under argon. The solution was heated without stirring during 2 h at 80 °C. After cooling down the solution, the suspension was centrifuged. The supernatant was eliminated and the solid washed with methanol to afford **POP-CorCo-DMSO**. The black powder was then washed with a solution of methanol saturated with ammonia to afford **POP-CorCo-1** coordinated by two NH_3 ligands on the cobalt center. The solid was then dried under vacuum at room temperature. Yield is 95% (104 mg). The characterization data are given in the SI.

Synthesis of POP-CorCo-2. Under inert atmosphere was dissolved cobalt corrole **3** (110 mg, 0.126 mmol, 1 eq) in tetrahydrofuran (40 mL) and gaseous ammonia was bubbling for 5 min in the solution affording a green solution. Then triethylamine (15 mL) and bis(triphenylphosphine)palladium(II) dichloride (7.1 mg, 0.010 mmol, 0.1 eq) were added. The mixture was heating under stirring at 70 °C and a solution of tetralkyne **1** (26.3 mg, 0.063 mmol, 0.5 eq) in tetrahydrofuran (30 mL) was added dropwise during at least 2 h. The solution was then allowed to stir for 24 h at 70 °C. After cooling down at room temperature, the black precipitate formed was filtered, washed with tetrahydrofuran followed by a saturated ammonia solution in tetrahydrofuran. The solid was dried under vacuum. Yield is 70 mg (70%). The characterization data are given in the SI.

Results and discussion

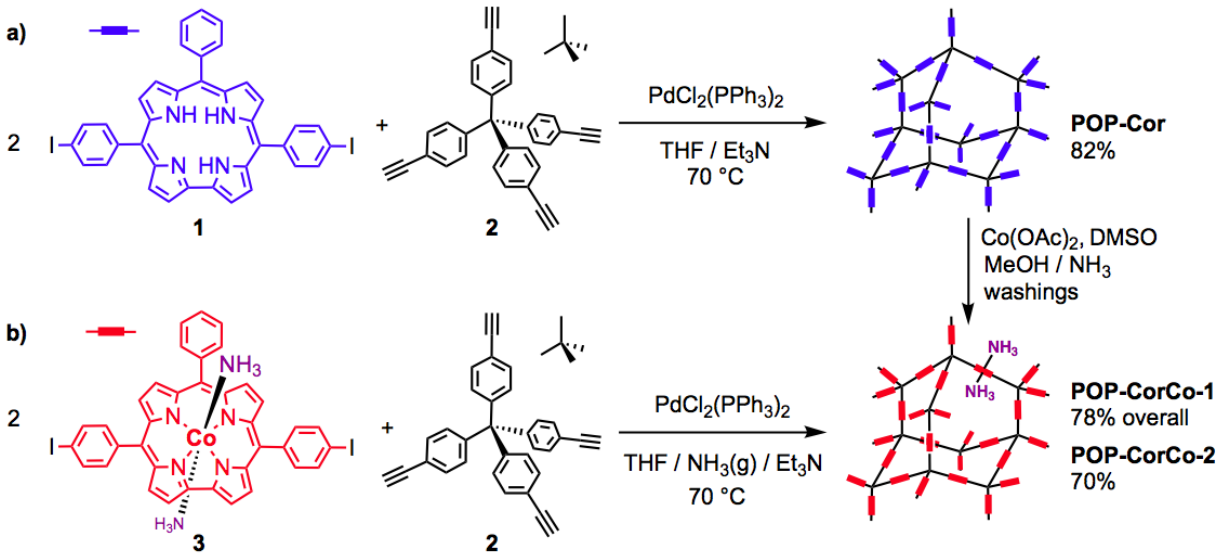
Synthesis and characterization

Hexacoordinated cobalt corrole complexes can be easily isolated and used in air atmosphere without any degradation when the coordination sphere of the metal center is fulfilled with two axial ligands like *e.g.* ammonia acting as a protecting group.[37] Interestingly, ammine ligands are sufficiently labile to be easily removed by gentle heating under vacuum to lead to the

"active" tetracoordinated cobalt corroles without any bound ligand in apical position. Such square planar complex constitutes the active species of cobalt corroles for CO bonding on the metal center.[34]

The incorporation of corrole macrocycles in a POP materials was motivated by their high internal surface area. The use of tetrahedral-shape building block were designed for 3D diamond-type assembly, in which carbon atoms are tetrahedral connected by covalent bonds, replacing C–C covalent bonds by rigid phenyl rings. Inspired by this concept, the first tetrahedral-shape POPs functionalized by corrole by coupling tetrakis(4-bromophenyl)methane **1** as the tetrahedral building units with the diiodocorroles **1** or **3** through the copper-free palladium-catalyzed Sonogashira coupling (also known as Heck alkynylation)[60,61] forming a three-dimensional extended structure based on the diamond topology with adamantane-like cages. In a first attempt, the free base corrole **3** was used as a linker (Scheme 1a). The coupling reaction was carried out without the use of copper(I) in order to avoid the complexation of the free base corrole by copper during the synthesis. The coupling reaction proceeded in tetrahydrofuran from which a black precipitate was deposited on the surface of the reaction flask after 24 h. The polymer **POP-Cor** thus obtained was found to be insoluble in usual organic solvents, unlike the corrole **1** and the tetrahedral building block **2**. The yield of **POP-Cor** was estimated at 82%.

The post-metalation procedure of **POP-Cor** was then carried out in DMSO using cobalt acetate. The penta-coordinated cobalt complexes formed with one coordinated DMSO molecule allow to stabilize the corrole complex. The washing of the solid with a solution of ammonia in methanol further exchanged DMSO by two labile ammine ligands to yield **POP-CorCo-1.** This exchange procedure allows to facilitate the regeneration of the tetra-coordinated active species for further CO binding studies.



Scheme 1 Schematic representation of two synthetic routes for preparing (a) **POP-CorCo-1** using a postmetalation and (b) **POP-CorCo-2** using a direct synthesis from the cobalt complex.

In order to compare the influence of the synthesis conditions on the porosity and CO adsorption properties, a second material **POP-CorCo-2** was also prepared starting from the bisammine cobalt corrole **3** instead of the free base, and the tetrahedral building block **1**. During the synthesis, the solution keeps a green colour characteristic of hexacoordinated cobalt corroles with two ammine ligands in axial position on the metal atom. The yield obtained for **POP-CorCo-2** is 70%.

Both materials are obtained as powder solids, and are insoluble in all common organic solvents. In order to determine the chemical composition of the materials and to give further evidence of the stoichiometric ratio between corroles and tetrahedral building units, we have used elementary analyzes (EA), dispersive energy analyzes (EDS), inductively coupled plasma spectroscopy (ICP), solid-state ^{13}C cross polarization-magic angle spinning nuclear magnetic resonance (CP/MAS NMR), Fourier transformation infrared (FTIR) and diffuse reflectance spectroscopy in the visible range.

The FTIR spectra of **POP-Cor** and the starting precursors show vibrational bands attributed to N–H, C≡C and C–H functional groups of the alkyne. The band corresponding to the N–H bond elongation is identified at 3371 cm^{-1} for the free base corrole **3** (Fig. 1). In the case of the tetrahedral compound **2**, two characteristic vibration bands of the alkyne functions are clearly shown at 3283 cm^{-1} and 2108 cm^{-1}, assigned respectively to the elongation of the C–H bond of the alkyne and to the elongation of the triple C≡C bond. The frequency of this latter band is characteristic of a terminal alkyne.[55,62]

FTIR spectra of **POP-Cor**, **POP-CorCo-1**, and **POP-CorCo-2** (Fig. S9) show an additional band at 2204 cm^{-1} corresponding to the vibration frequency of the C≡C bond for the disubstituted alkyne. This band gives further evidence of the alkyne coupling between precursors **2** and the corroles **1** or **3** thanks to Sonogashira coupling reaction. The FTIR spectra in the 2050-2300 cm^{-1} region is in perfect agreement with the previous results obtained on microporous conjugated polymers (CMPs) also obtained by Sonogashira coupling.[63,64]

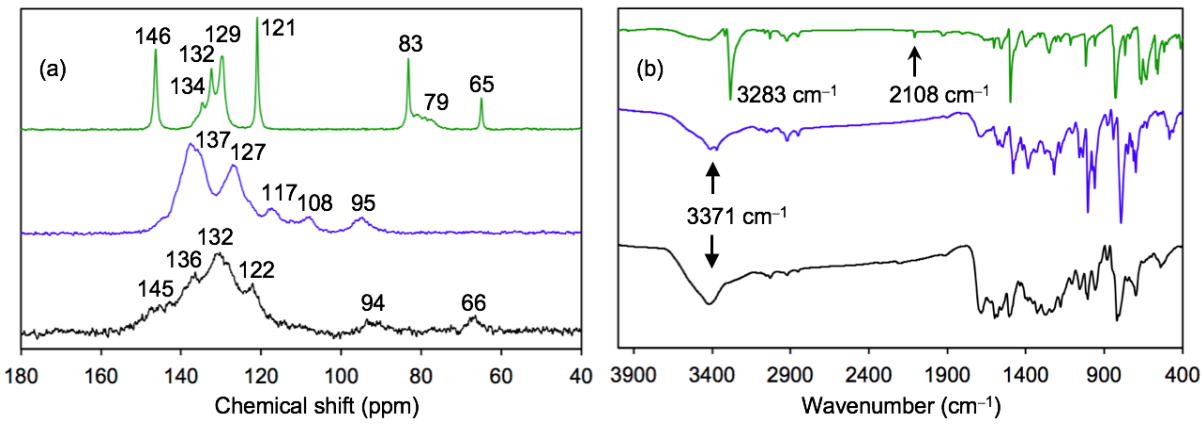


Fig. 1 (a) ^{13}C CP/MAS NMR spectra and (b) FTIR spectra of compounds of **2** (green line), free base corrole **1** (blue line), and **POP-Cor** (black line).

However, the vibration band at 2108 cm^{-1} corresponding to the frequency of elongation of the terminal alkyne is still observed (Fig. S9), mainly for **POP-CorCo-2**. The presence of this

band indicates that the coupling between the terminal alkyne of the tetrahedron and the corroles **1** and **3** is not fully achieved.

Solid-state ^{13}C CP/MAS NMR spectroscopy was also used to confirm the formation of the polymer and provides information on its structure. For comparison and interpretation purposes, corrole **1** and tetralkyne **2** were also analyzed both in solution and in the solid state. The polymerization reaction can be monitored by focusing on the chemical shifts of the carbon atom bound to iodine atom for **1** and those of the alkyne function in the case of **2**. The univocal attribution of these signals is described in the Supporting Information (Fig. S3).

^{13}C CP/MAS NMR spectrum of the tetrahedral-shape alkyne **2** is similar to the spectrum observed in solution, as shown in Fig. 1 and Fig. S2–S3, with the exception of the signal at 79 ppm corresponding to the carbon atom of the terminal *C*-alkyne that gives a large signal. Corrole **1** displays only four broad signals between 108 and 137 ppm due to overlap of the aromatic carbon resonance. More importantly, the broad signal at 95 ppm is clearly assigned to the carbon atom bearing the iodine atom. **POP-Cor** shows at least four signals between 122 and 145 ppm which overlap to form a broad signal as observed for starting corrole **1**. The signals at 132 and 136 ppm are attributable to the overlap of signals belonging to both **2** and **1** while the two other signals at 122 and 145 ppm are only assigned to the building block **2**, including the signal at 66 ppm characteristic of the methine carbon of **2**. In addition, no signal corresponding to the terminal and quaternary alkyne, expected at 79 and 83 ppm, is shown but instead a broad signal at 94 ppm is observed. The latter signal seems to indicate that the heterocoupling reaction between the **2** and **1** building blocks is not fully quantitative. These results are in agreement with the FTIR data presented above.

It should be noted that multiple covalent structures can be generated due to the numerous possible pathways of 3D growing of the network. Therefore, crystallization of POP is not possible when the coupling reactions used are irreversible. That leads to disordered kinetic

products that are amorphous since self-healing and error correction cannot occur during the precipitation/crystallization. As a result, PXRD analysis of the POPs reveals only the formation of amorphous structures.

UV-visible spectrum (Fig. S10) of free base corrole **1** recorded in toluene solution displays a characteristic Soret band at 424 nm and three main Q bands at 568, 622 and 653 nm. UV-visible solid-state spectrum measured in diffuse reflectance mode recorded for this complex shows a Soret band at 425 nm and two broad bands at 594 and 650 nm. In the solid state, the free base **POP-Cor** displays a bathochromic shift of the broad Soret band at 470 nm and two broad Q bands at 603 and 670 nm, which confirms the incorporation of free base corrole in the material. The 45 nm bathochromic shift of the Soret band can be explained by π-stacking interactions between adjacent corroles in the material[65] when compared to the free base precursor **1**. This result strongly suggests the formation of aggregated corroles in the solid indicating that the network is probably interpenetrated (see below).

Concerning the cobalt corrole, UV-visible spectrum recorded in solution for the bis-ammine corrole **3** exhibits a split Soret band at 438 and 455 nm as well as three Q bands at 540, 586 and 632 nm (Fig. 2). The spectral morphology and position of the Q bands are characteristic of hexa-coordinated cobalt corroles.[37] UV-visible spectrum recorded in solid state for this corrole displays a broad and split Soret band at 408 nm and 444 nm, and three Q bands at 535, 596 and 644 nm. The diffuse reflectance spectrum of **POP-CorCo-2** shows a weak Soret band at 467 nm but two intense and well-defined Q bands at 605 and 657 nm. The small bathochromic displacement of these bands (~ 10 nm) and their shape are in agreement with the hexacoordination of cobalt corroles for **POP-CorCo-2** with no degradation of the complexes during the material synthesis.

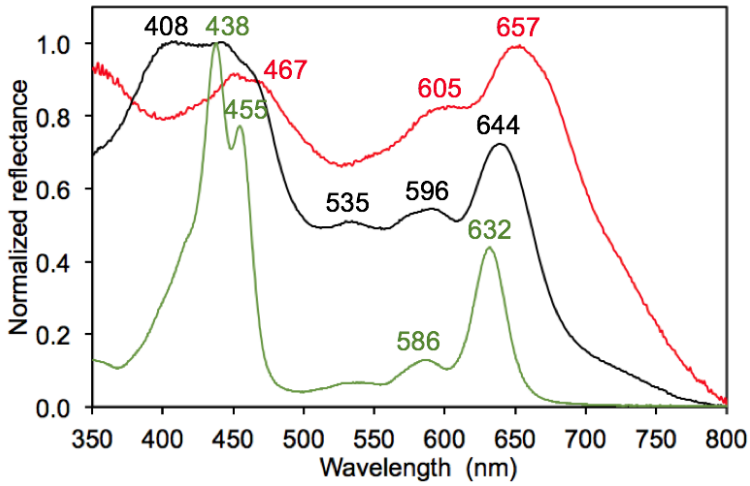


Fig. 2 UV-visible spectra for corrole **3** recorded in solution (green line) and in solid state (black line), and for **POP-CorCo-2** (red line) showing evidence of the hexa-coordination of the cobalt center.

The morphology and composition of **POP-Cor** and their metalated counterparts were also analyzed by transmission electron microscopy (TEM) and electron microscopies (SEM) coupled with Energy Dispersive X-ray Spectrometry (EDS). Surprisingly, regular spherical-shape nanoparticles with a narrow size distribution was revealed, although non-structural conditions were used (Fig. 3). The smooth nanospheres present an average size in the range 800-1000 nm for **POP-Cor** and **POP-CorCo-1**. Interestingly, the morphology and particle size remain unchanged after insertion of cobalt in the corrole core (**POP-CorCo-1**), that means after post-metalation of the **POP-Cor** in the DMSO followed by ammonia treatment. This observation is obviously resulting from the porosity of the material, showing that the diffusion of the metallic salt is not hindered to reach free base corroles. In addition, **POP-CorCo-2** presents the same nanosphere morphology with slightly smaller and rougher particules (500–700 nm). Transmission electron microscopy (TEM) images (Fig. S11) also reveal that the POPs are obtained in the form of sphere-like nanoparticles with domain sizes of 800-1000 nm and demonstrate uniform distribution of the elements, in accordance with the SEM analyses. In addition, TEM images show that the spherical morphology of the corrole-

based POPs cannot be attributed to a heterogeneous nucleation mechanism involving palladium nanoparticles since this metal is homogenously distributed inside the nanospheres. Hence, the homogeneous contrast thus observed indicates on one hand the absence of palladium core shell particles and on the other hand reveals that the nanospheres are filled. The nucleation of the particles is thus mainly due to the solubility decrease of the polymerization products and not to a nucleation phenomenon induced by palladium nanoparticles.

EDS analyses (Table S1) confirm the presence of N and Co elements in the **POP-CorCo** polymers as well as traces of palladium and phosphorous atoms resulting from the catalyst. The P/Pd ratio for the three materials are close to 2 in agreement with the $PdCl_2(PPh_3)_2$ catalyst used, which shows that the by-products (*e.g.* phosphine oxide, Pd^0 particles) are trapped inside the material and are not removed by washing. EDS also revealed the presence of residual iodine brought by the corrole precursors **1** and **3**. This last result gives evidence that the cross-linking polymerization reaction is not fully achieved. This fact is in agreement with the ^{13}C CP/MAS data since signal attributed to the C–I bond was highlighted.

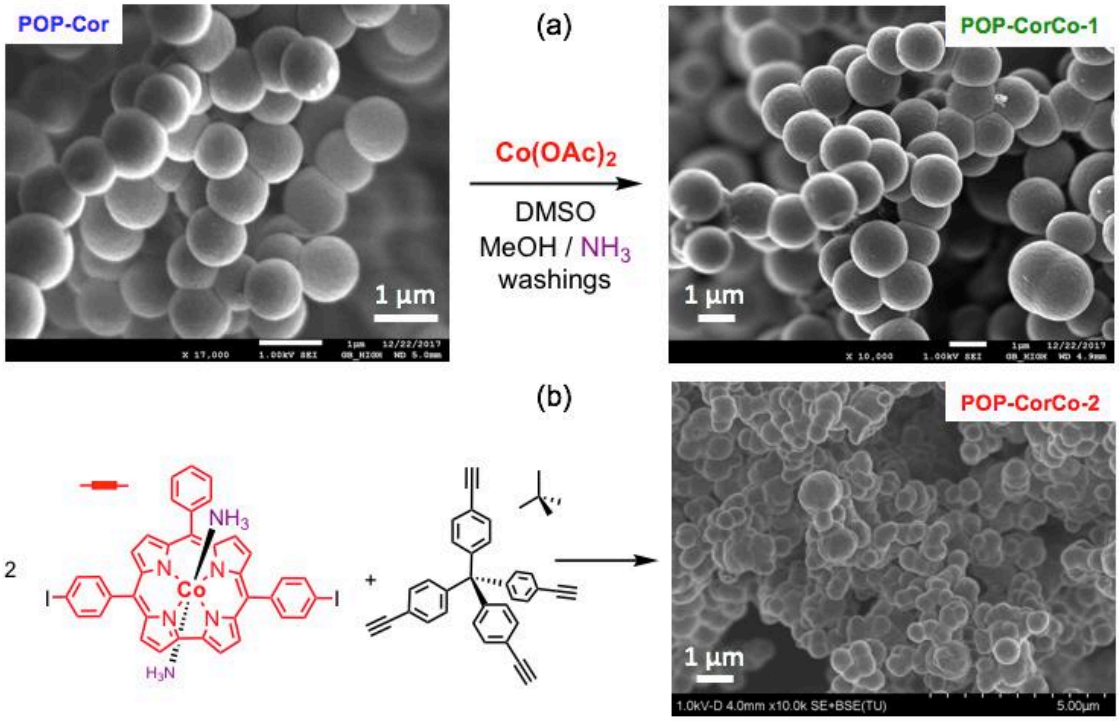


Fig. 3 SEM images of (a) **POP-Cor** (top left), **POP-CorCo-1** (top right) and (b) **POP-CorCo-2** (bottom right).

Related to these data, effective chemical formulas were proposed for each material based on elementary and ICP analyses, which gave the amount of metals (Co, Pd) and organic part in each material (see synthetic part in SI). The proposed elemental composition is based on a 2:1 reaction between the corrole moiety and the tetratopic tetrakis(ethynylphenyl)methane linker. However, as suggested by other authors,[63] some discrepancies between the elemental analyses values and those expected based on the copolymerization stoichiometry can arise from remaining the halogen atoms in the chain termination and, possibly, homo-coupling between the tetra-alkyne linker units itself. Nevertheless, the ICP and EDS analyses confirmed the expected metal content, the N/metal ratio and the presence of residual iodine atoms. The results are therefore in fairly good agreement with a 2:1 ratio of corrole over tetrahedral building unit.

Thermal stability

Prior to gas adsorption measurements, thermogravimetric analyses (TGA) were conducted between 25 to 800 °C under an oxidant atmosphere to evaluate the thermal stability of the **POP-Cor** materials (Fig. S12). The TGA curve for **POP-Cor** shows an oxidation step between 200 °C and 300 °C followed by calcination that occurs on a large temperature range between 300 and 580 °C. A plateau is then reached at 6% corresponding to palladium residues used for the Sonogashira cross-coupling. As shown by EDS analyses, Pd precipitates as nanoparticles during the synthesis and cannot be removed from samples by washings. For **POP-Cor-1** and **-2**, ammonia molecules coordinated to the cobalt atoms are lost in the range 25–130 °C, and the 3% weight loss agrees with two ammonia ligands *per* cobalt atom (calcd: 2.1%) and with the presence of small amount of adsorbed water in the porous framework. Further weight loss between 260-460 °C is attributed to the calcination of the organic part of

the materials. A plateau is then reached at 12% and 8.3% for **POP-Cor-1** and **-2**, respectively, in fairly good agreement with the expected amount of cobalt oxide and palladium residues (calcd for CoO: 9.3%). Interestingly, the similitude between both thermograms shows that the two synthetic pathways for preparing cobalt corrole materials gave analogous frameworks with similar thermal stability.

Porosity of the POPs

In order to examine the permanent porosity of the POPs, nitrogen adsorption-desorption measurements were performed at 77 K. Prior to the gas adsorption measurements, materials were evacuated at 80 °C for at least 3 h until the pressure reached 5 10^{-5} atm, generating the fully desolvated materials. **POP-Cor** displays a near-reversible type-I sorption behavior[66] with high nitrogen uptake at low relative pressure and an adsorbed amount of 228.0 $cm^3\ g^{-1}$ (STP) at 1 atm revealing their microporous characters. However, at relative pressure higher than 0.1 the adsorption branch shows a gradual uptake up to 1 atm, indicating a significant contribution of small mesopores (Fig. 4). In addition, the fact that the desorption isotherm does not perfectly fit the adsorption one indicates the existence of defects and irregular pores in size and shape. According to the N_2 adsorption isotherm, the Brunauer-Emmett-Teller (BET) surface area and the pore volume were estimated to 645 $m^2\ g^{-1}$ and 0.352 $cm^3\ g^{-1}$, respectively (see also Fig. S13).

For the metalated **POP-CorCo-1** and **2**, the type-I adsorption isotherms confirmed their permanent porosity and microporosity. Interestingly, the two materials present similar porosities despite the fact that two different synthetic pathways were used. Indeed, the BET surface areas and pore volumes are 513 $m^2\ g^{-1}$, 0.245 $cm^3\ g^{-1}$, 436 $m^2\ g^{-1}$ and 0.235 $cm^3\ g^{-1}$ for **POP-CorCo-1** and **POP-CorCo-2**, respectively. These results give some evidence of the analogous structure of these two materials.

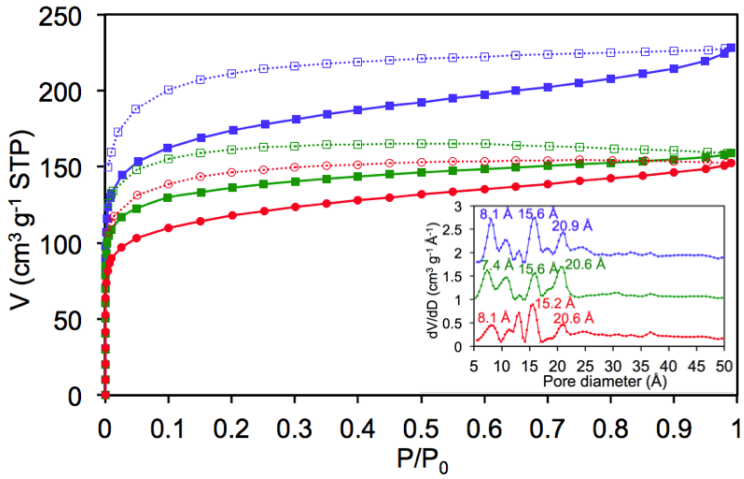


Fig. 4 N_2 adsorption (closed symbols) and desorption (open symbols) isotherms recorded at 77 K for **POP-Cor** (blue square), **POP-CorCo-1** (green square) and **POP-CorCo-2** (red circles). Insert shows the respective pore size distribution curves calculated using NLDFT method.

The pore size distribution curves (PSD) for the corrole polymer networks calculated using nonlocal density functional theory (NLDFT) reveals the presence of micropores and small mesopores as well as irregularities in the structures, revealed by the non-coincidence of the adsorption and desorption branches. All the polymers exhibit abundant micropores and quite inhomogeneous structures with mean peaks found at around 8, 10, 13, 15 and 20 Å. No significant PSD difference was observed for the three materials, which reveals their structural similarity as previously shown by SEM and TEM analyses. These results demonstrate that the synthetic route used does not play a major role in the generation of porous architectures and the structural properties are mainly directed by the topology of the tetrahedral building block. In addition, the pore size was estimated based on a geometrical construction for a regular and non-interpenetrated structure (Fig. S17). As a result, the size of the trigonal prism included in the cavity was calculated to 81 x 50 Å and the sphere size that perfectly fit the cavity was estimated to about 30 Å. The main explanation of the difference between the observed and calculated pore size is the existence of a smaller, secondary pore cavity. These findings

support the fact that interpenetrated networks are formed whatever the starting corrole used, leading to a significant decrease of the pore size.

Actually, when tetrahedra are directly connected together, the structure obtained adopts a non-interpenetrated diamond-like topology as observed for MOFs[67,68] and COFs.[55,69] However, it has been shown for these two families of materials that when tetrahedral nodes are separated by long rod-like linkers, the resulting structures are often interpenetrated.[57,70,71] Considering that the corrole linker can be seen as a cylinder of about 18 Å long, the formation of a multi-interpenetrated structure is quite obvious and expected as previously observed in other porous polymers.[57]

The porosity of other POPs built with porphyrin are known to vary between 156 and 1711 $m^2 g^{-1}$ depending upon the nature of the spacers.[72,73] However, architectures built from difunctionalized aryl porphyrins are still scarce and, to the best of our knowledge, only one example has been described with a similar porosity than the two POP-CorCo described herein.[74]

Gas adsorption properties

Considering the porous structures decorated with cobalt corroles, their potential application for adsorption of CO and other gases present in the atmosphere such as N_2, O_2 and CO_2 was further investigated in order to highlight the selectivity for CO adsorption. As shown in Fig. 5 and Tables S3-S5, the adsorption isotherms for these gases recorded at 298 K indicate that compounds **POP-CorCo-1** and **-2** present different gas adsorption amounts. At 1 atm, the two materials display a CO uptake of 23.5 $cm^3 g^{-1}$ and 23.7 $cm^3 g^{-1}$ at 298 K, respectively. CO adsorption at low pressure (< 0.01 atm) is dominated by a selective sorption thanks to binding between CO molecules and the unsaturated site of the metallocorroles in the apical position of the cobalt atoms. At higher pressures the highly energetic unsaturated metal sites become

fully occupied with CO molecules and physisorption starts to dominate the adsorption process.

The uptake capacities are lower than some benchmark MOFs with high density of open metal sites, for instance, M-MOF-74 (M = Mg: 97 $cm^3\ g^{-1}$; M = Fe: 132 $cm^3\ g^{-1}$) and HKUST-1 (32 $cm^3\ g^{-1}$) at 1 atm and 298 K but they lack selectivity towards O_2.[31,75] However, to our knowledge, no POP have been described for the selective adsorption of CO. As expected, **POP-CorCo-1** and **-2** exhibit small amounts of N_2 (9.1 and 8.5 $cm^3\ g^{-1}$) and O_2 (8.1 and 4.6 $cm^3\ g^{-1}$) uptake, respectively, in the same conditions. A higher CO_2 capture was observed (32.5 and 27.9 $cm^3\ g^{-1}$), ascribed to stronger interactions between the surface and CO_2 compared to CO, N_2 and O_2 thanks to its high quadrupole moment (13.4 x 10^{-40} C m^2) that enhances adsorbent-adsorbate interactions through a physisorption process.[76-79] Therefore, while pressures increase, there is a detrimental impact on CO/CO_2 selectivity as lower energetic dispersion forces dominate and reduce the overall impact of previously dominant chemical interactions.

The adsorption isotherms were also recorded for the non-metalated **POP-Cor**, that showed obviously very low affinity for N_2, O_2 and CO_2 as well as CO (Fig. S20). Hence only non-selective adsorbent-adsorbate interactions through a physisorption process occurred. This result gives evidence of the coordination of CO on the cobalt atoms in **POP-CorCo-1** and **-2** as already observed for the bulk complexes.[33,34]

To express the adsorption behavior of the pure components, the isotherm data were fitted with a triple-site Langmuir model for best describing CO adsorption[55,80] while a single-site Langmuir model enables to fit the CO_2, N_2 and O_2 adsorption isotherms. The calculated isotherms allow us to estimate half saturation pressure for the selective sorption process of 0.66 x 10^{-3} atm and 0.92 x 10^{-3} atm (Table S4) for **POP-CorCo-1** and **-2**, respectively, giving further evidence of the high affinity of the materials for CO. However, the amount of cobalt

active site was evaluated to only 23 and 30% (Table S3). Actually, although POPs are known to be potential candidates for metal ion binding[81,82] or gas adsorption[43,46] thanks to their porosity and their versatile synthesis, the performances of our materials are lessened by buried chelating sites stemmed from the small and irregular pores as well as interpenetration of the framework.

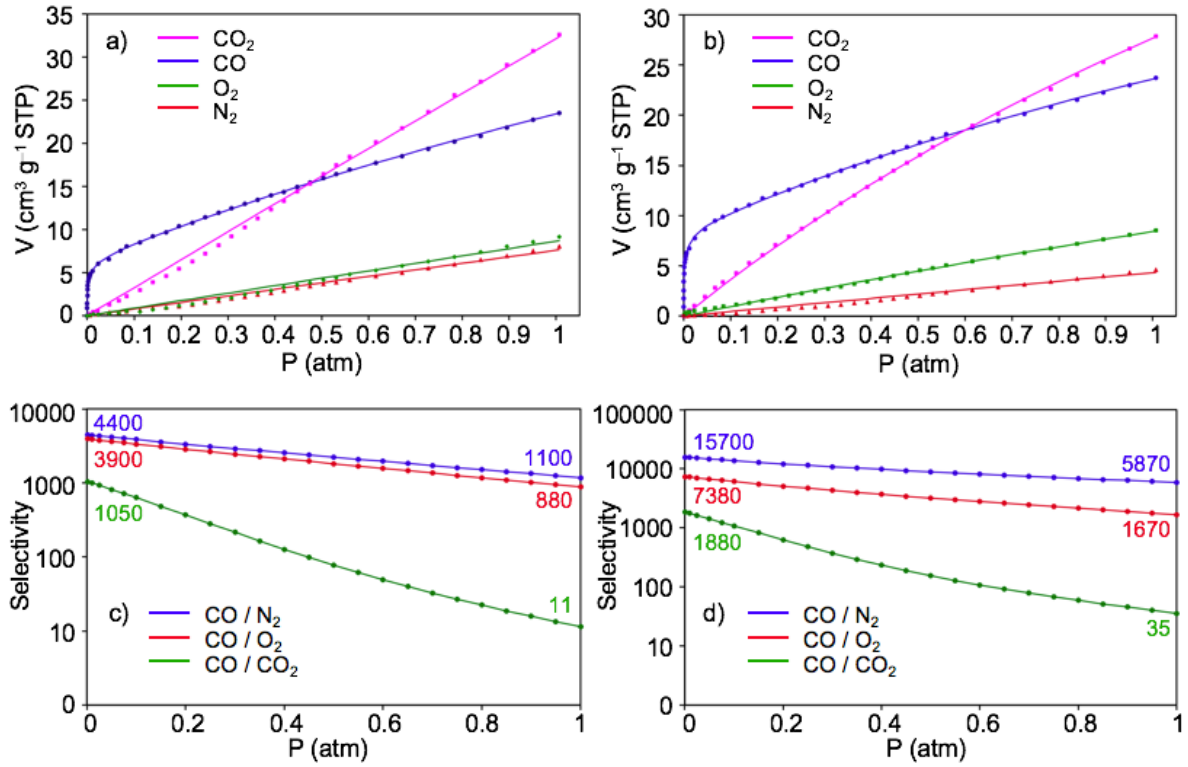


Fig. 5 Adsorption isotherms of CO (blue symbols), CO_2 (pink symbols), N_2 (red symbols) and O_2 (green symbols) recorded at 298 K for (a) **POP-CorCo-1** and (b) **POP-CorCo-2**. Solid lines represent fitting curves using a single-site Langmuir model for N_2, O_2 and CO_2, and a triple-site Langmuir model for CO (see equations (1) and (2) and Tables S3–S5 in ESI). (c) and (d) IAST selectivity calculations at 298 K of CO over CO_2, N_2 and O_2 for (c) **POP-CorCo-1** and (d) **POP-CorCo-2** assuming a 0.01:99.99 mixture (100 ppm CO in N_2, O_2 or CO_2).

The fitting parameters obtained for the multisite Langmuir model allow to determine selectivities for CO over CO_2, N_2 and O_2 using IAST calculations, considering a gas mixture containing 100 ppm of CO in the other gases (Fig. 5 (c), (d) and Table S6).[76,80] These conditions were chosen in order to estimate the potential application of these materials in a

real atmosphere, that means in which these compounds would be likely to be exposed for CO detection. The calculations gave very high selectivity values for CO over N_2 and O_2 of 4400, 3900, 15700 and 7380 at zero pressure for **POP-CorCo-1** and **-2**, respectively. These values correspond to the ratio of their corresponding Henry constants at zero pressure. The selectivities decrease gradually with increasing the pressure but remain higher than 1000 at 1 atm. It is worth noticed that **POP-CorCo-2** showed the highest selectivities whatever the gas and the pressure considered, probably owing to a better accessibility of the cobalt site for CO binding. We would like to emphasize that the selectivity for CO over N_2 and CO_2 is far higher than those reported for other porous materials like MOF and POP.[31,75]

However, CO/CO_2 selectivity values at low coverage are 1050 and 1880 for **POP-CorCo-1** and **-2**, respectively, and are significantly lower than values calculated over N_2 and O_2. and the selectivities decrease quite significantly as the pressure increases. However, in a real atmosphere containing 400 ppm of CO_2, only the selectivity at low partial pressures of CO_2 are to be considered for application as gas sensors.

Stability and reversibility studies were also performed for **POP-CorCo-1** (Fig. S21). Three successive CO adsorption cycles of CO adsorption were carried out on this material after degassing at 80 °C after each sorption step. The results showed that the adsorption properties are preserved after each cycle thus demonstrating the stability of the material. It should be emphasized that O_2 adsorption isotherm was measured after the first CO adsorption, which highlights the stability of the cobalt corrole complex once immobilized in the organic matrix. Indeed, no oxidation of the tetracoordinated cobalt complex was observed.[37]

The reversibility of the carbon monoxide adsorption on **POP-CorCo-2** was also carried out by FTIR spectroscopy under vacuum and CO atmosphere (Fig. 6). A blank measurement was realized after degassing the pellet in the environmental chamber for at least 24 h in view to remove the ammine coordinated on the metal. After exposure to CO (1 bar) during 1 h, the

pellet was evacuated for 1 min before recording the first spectrum (Fig. 6a), and successive measurements were then run each 2 h (Fig. 6b). After CO exposure, the spectrum shows an intense vibration band at 2046 cm^{-1} and this frequency value is characteristic of the elongation of the C≡O triple bond when CO is bound to a metal ion *via* the carbon atom. When carbon monoxide bind to a transition metal, the bonding interactions involves synergic σ-donation from the carbon lone-pair 5s orbital to the metal along with π-backdonation of electron density from the metallic d_{xz}, d_{yz} orbitals in the 2p* antibonding orbitals of CO.[83-86] The π-backdonation tends to weaken the CO bond leading to a red-shift of the CO stretching toward lower frequencies with respect to free CO (2143 cm^{-1}), as already observed in a Co(III) corrole series.[34,87]

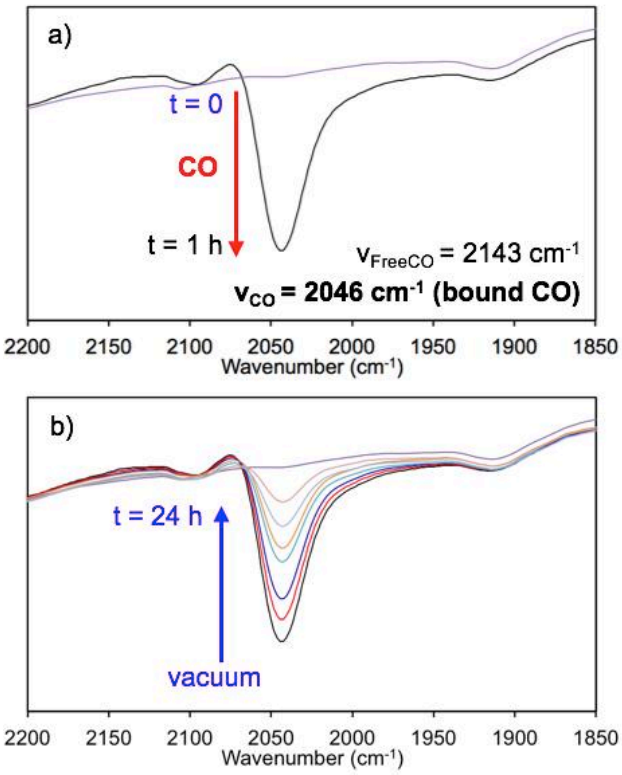


Fig. 6 FTIR monitoring of the adsorption/desorption process recorded for **POP-CorCo-2** (a) after 24 h evacuation at 2 mbar (blue line) followed by CO exposure for 1 h and (b) during desorption under vacuum (1 min→24 h).

During degassing of the pellet sample, a gradual decrease of the CO vibration intensity is observed and this band almost disappears after 24 h. These data clearly reveal that CO adsorption in the polymers involved the coordination of the gaseous molecules on the cobalt atom according to a reversible process.

FTIR spectra were also recorded for **POP-CorCo-2** in CO/CO_2 gas mixture containing 100 ppm of CO. After gas exposure, the spectrum shows a vibration band at 2057 cm^{-1} characteristic of the CO bound to the metal ion (Fig. S23). This vibration band is slightly blue-shifted compared to the CO stretching observed with neat CO but is significantly red-shifted toward lower frequencies with respect to free CO (2143 cm^{-1}) due to the π-back-donation effect. After degassing, this band totally vanishes in less than 25 min. It is thus clearly shown than CO binding occurs reversibly, even when the gas mixture contains very low concentration of CO (100 ppm).

The efficient sensing of CO in a polluted environment requires advanced sorbent materials with not only high binding affinity and selectivity but also fast kinetic sorption. Kinetic studies have been performed in static conditions at 298 K and at low coverage. The samples were previously degassed for 2 h before measurements and adsorption kinetics were recorded during at least 6 min (Fig. S22). Whatever the pressure range, the half-saturation time for **POP-CorCo-1** and **-2** is short, typically between 6 and 16 s, and the saturation plateau is rapidly reached, even for lower coverage (less than 100 ppm). Such short response times and room-temperature CO sensing capabilities are highly outstanding compared to other reported CO sensors.[13,88] These results strongly suggest that highly attractive gas sensing properties can be achieved porous polymers functionalized with cobalt corroles.

Conclusion

In summary, we report herein a highly versatile and effective methodology to easily synthesize shape microspherical porous organic polymer based on cobalt corroles able to bind carbon monoxide. Two synthetic strategies have been used for preparing materials. It was evidenced that the use of bis-ammine protected metallocorrole gave a material with better CO sorption performance. The functionalized polymers exhibit a high permanent porosity and an outstanding affinity and selectivity for CO binding over N_2, O_2 and CO_2 compared to other porous materials (MOFs, COFs). Interestingly, the coordination of CO on cobalt is fully reversible and fast kinetic were also observed. The immobilization of cobalt corrole in a porous POP gave access to new materials designed for the selective carbon monoxide adsorption and detection with respect to other gases present in the atmosphere. Our results demonstrated that incorporation of highly reactive complexes in a porous POP framework provides an appealing strategy for designing selective CO capture featuring great potential for developing new gas sensor devices. Hence, devices built with these polymeric sensors should outperform those found in the market place since the current sensors are highly disturbed by the presence of other gases. The reliability of the response and the robustness of the sensors are also crucial parameters for sensing applications. In addition, one of the main problem is to elaborate sensors able to work in the presence of humidity. Functionalization of hydrophobic polymers with corroles should give a good opportunity to solve this problem. Our work is still underway to determine the CO sensing response of our polymers in humid conditions.

Conflicts of interest

The authors declare no conflict of interest.

Acknowledgements

This work was supported by the CNRS (UMR UB-CNRS 6302), the "Université Bourgogne Franche-Comté", the FEDER-FSE Bourgogne 2014/2020 (European Regional Development Fund), the Conseil Régional de Bourgogne (CRB) through the "Plan d'Actions Régional pour l'Innovation" (PARI II CDEA project) and the JCE program. V.Q. warmly thanks CRB for PhD grant. ANR is also acknowledged for financial support (CO^3SENS). The authors wish also to warmly thank Frédéric Herbst and Dr. Rémi Chassagnon (Laboratoire Interdisciplinaire Carnot de Bourgogne) for SEM and TEM analyses.

References

1. M. Braubach, A. Algoet, M. Beaton, S. Lauriou, M. E. Heroux and M. Krzyzanowski, *Indoor Air*, 2013, **23**, 115-125.
2. A. L. Chiew and N. A. Buckley, *Critical Care*, 2014, **18**, 221-229.
3. J. P. Collman and L. Fu, *Acc. Chem. Res.*, 1999, **32**, 455-463.
4. T. Omura and R. Sato, *J. Biol. Chem.*, 1964, **239**, 2370-2378.
5. M. F. Perutz, *Annu. Rev. Physiol.*, 1990, **52**, 1-26.
6. B. A. Springer, S. G. Sligar, J. S. Olson and G. N. Phillips, Jr., *Chem. Rev.*, 1994, **94**, 699-714.
7. S. R. Thorn and L. W. Keim, *J. Toxicol., Clin. Toxicol.*, 1989, **27**, 141-156.
8. "*WHO guidelines for indoor air quality: selected pollutants*", 2010.
9. J. J. Baschuk and X. Li, *Int. J. Energy Res.*, 2001, **25**, 695-713.
10. A. A. Franco, M. Guinard, B. Barthe and O. Lemaire, *Electrochim. Acta*, 2009, **54**, 5267-5279.
11. Y. Lee and J. Kim, *Anal. Chem.*, 2007, **79**, 7669-7675.
12. H. Kim, C.-S. Park, K.-M. Kang, M.-H. Hong, Y.-J. Choi and H.-H. Park, *New J. Chem.*, 2015, **39**, 2256-2260.
13. X. Zhou, S. Lee, Z. Xu and J. Yoon, *Chem. Rev.*, 2015, **115**, 7944-8000.
14. D. Degler, S. A. Müller, D. E. Doronkin, D. Wang, J.-D. Grunwaldt, U. Weimar and N. Barsan, *J. Mater. Chem. A*, 2018, **6**, 2034-2046.

15. J. L. Solis, L. B. Kish, G. Seeton, F. Green, G. Iannaccone, L. B. Kish and J. R. Vig, *Proc. SPIE Int. Soc. Opt. Eng.*, 2003, **5115**, 211-217.
16. N. Bârsan and U. Weimar, *J. Phys.: Condens. Matter.*, 2003, **15**, R813.
17. A. Burresi, A. Fort, S. Rocchi, B. Serrano, N. Ulivieri and V. Vignoli, *Sens. Actuators B, Chem*, 2005, **106**, 40-43.
18. F. Rock, N. Barsan and U. Weimar, *Chem. Rev.*, 2008, **108**, 705-725.
19. T. Nandy, R. A. Coutu, Jr. and C. Ababei, *Sensors*, 2018, **18**, 3443-3472.
20. C. Marin-Hernandez, A. Toscani, F. Sancenon, J. D. Wilton-Ely and R. Martinez-Manez, *Chem. Commun.*, 2016, **52**, 5902-5911.
21. M. E. Moragues, J. Esteban, J. V. Ros-Lis, R. Martinez-Manez, M. D. Marcos, M. Martinez, J. Soto and F. Sancenon, *J. Am. Chem. Soc.*, 2011, **133**, 15762-15772.
22. M. E. Moragues, R. Montes-Robles, J. V. Ros-Lis, M. Alcañíz, J. Ibañez, T. Pardo and R. Martínez-Máñez, *Sens. Actuators B*, 2014, **191**, 257-263.
23. M. E. Moragues, A. Toscani, F. Sancenón, R. Martínez-Máñez, A. J. P. White and J. D. E. T. Wilton-Ely, *J. Am. Chem. Soc.*, 2014, **136**, 11930-11933.
24. A. Toscani, C. Marin-Hernandez, M. E. Moragues, F. Sancenon, P. Dingwall, N. J. Brown, R. Martinez-Manez, A. J. White and J. D. Wilton-Ely, *Chem. Eur. J.*, 2015, **21**, 14529-14538.
25. J. Jiang, Y. Zhao and O. M. Yaghi, *J. Am. Chem. Soc.*, 2016, **138**, 3255-3265.
26. S. M. J. Rogge, A. Bavykina, J. Hajek, H. Garcia, A. I. Olivos-Suarez, A. Sepulveda-Escribano, A. Vimont, G. Clet, P. Bazin, F. Kapteijn, M. Daturi, E. V. Ramos-Fernandez, I. X. F. X. Llabres, V. Van Speybroeck and J. Gascon, *Chem. Soc. Rev.*, 2017, **46**, 3134-3184.
27. Y. Zeng, R. Zou and Y. Zhao, *Adv. Mater.*, 2016, **28**, 2855-2873.
28. D. A. Reed, D. J. Xiao, M. I. Gonzalez, L. E. Darago, Z. R. Herm, F. Grandjean and J. R. Long, *J. Am. Chem. Soc.*, 2016, **138**, 5594-5602.
29. M. I. Gonzalez, J. A. Mason, E. D. Bloch, S. J. Teat, K. J. Gagnon, G. Y. Morrison, W. L. Queen and J. R. Long, *Chem. Sci.*, 2017, **8**, 4387-4398.
30. H. Li, K. Wang, Y. Sun, C. T. Lollar, J. Li and H.-C. Zhou, *Mater. Today*, 2018, **21**, 108-121.
31. A. Evans, R. Luebke and C. Petit, *J. Mater. Chem. A*, 2018, **6**, 10570-10594.
32. J.-R. Li, R. J. Kuppler and H.-C. Zhou, *Chem. Soc. Rev.*, 2009, **38**, 1477-1504.
33. J. M. Barbe, G. Canard, S. Brandès and R. Guilard, *Chem. Eur. J.*, 2007, **13**, 2118-2129.

34. J.-M. Barbe, G. Canard, S. Brandès, F. Jerôme, G. Dubois and R. Guilard, *Dalton Trans*., 2004, 1208-1214.
35. X. Sheng, H. Zhao and L. Du, *Sci*. *Rep*., 2017, **7**, 14536-14546.
36. M. Vanotti, C. Theron, S. Poisson, V. Quesneau, M. Naitana, V. Soumann, S. Brandès, N. Desbois, C. P. Gros, T.-H. Tran-Thi and V. Blondeau-Patissier, *Proceedings*, 2017, **1**, 444-447.
37. V. Quesneau, W. Shan, N. Desbois, S. Brandès, Y. Rousselin, M. Vanotti, V. Blondeau-Patissier, M. Naitana, P. Fleurat-Lessard, E. Van Caemelbecke, K. M. Kadish and C. P. Gros, *Eur*. *J*. *Inorg*. *Chem*., 2018, **38**, 4265-4277.
38. S.-Y. Ding, M. Dong, Y.-W. Wang, Y.-T. Chen, H.-Z. Wang, C.-Y. Su and W. Wang, *J*. *Am*. *Chem*. *Soc*., 2016, **138**, 3031-3037.
39. H. M. El-Kaderi, J. R. Hunt, J. L. Mendoza-Cortes, A. P. Côté, R. E. Taylor, M. O'Keeffe and O. M. Yaghi, *Science*, 2007, **316**, 268-272.
40. P. J. Waller, F. Gandara and O. M. Yaghi, *Acc*. *Chem*. *Res*., 2015, **48**, 3053-3063.
41. M. G. Rabbani and H. M. El-Kaderi, *Chem*. *Mater*., 2012, **24**, 1511-1517.
42. H. Ma, H. Ren, X. Zou, F. Sun, Z. Yan, K. Cai, D. Wang and G. Zhu, *J*. *Mater*. *Chem*. *A*, 2013, **1**, 752-758.
43. L. Zou, Y. Sun, S. Che, X. Yang, X. Wang, M. Bosch, Q. Wang, H. Li, M. Smith, S. Yuan, Z. Perry and H.-C. Zhou, *Adv*. *Mater*., 2017, **29**, 1700229.
44. B. Zhang, J. Yan and Z. Wang, *J*. *Phys*. *Chem*. *C*, 2018, **122**, 12831-12838.
45. W. Wang, M. Zhou and D. Yuan, *J*. *Mater*. *Chem*. *A*, 2017, **5**, 1334-1347.
46. G. Kupgan, L. J. Abbott, K. E. Hart and C. M. Colina, *Chem*. *Rev*., 2018, **118**, 5488-5538.
47. M. S. Lohse and T. Bein, *Adv*. *Funct*. *Mater*., 2018, **28**, 1705553.
48. G. Lin, H. Ding, D. Yuan, B. Wang and C. Wang, *J*. *Am*. *Chem*. *Soc*., 2016, **138**, 3302-3305.
49. Q. Gao, X. Li, G.-H. Ning, K. Leng, B. Tian, C. Liu, W. Tang, H.-S. Xu and K. P. Loh, *Chem*. *Commun*., 2018, **54**, 2349-2352.
50. Z. Li, Y. Zhang, H. Xia, Y. Mu and X. Liu, *Chem*. *Commun*., 2016, **52**, 6613-6616.
51. S. Lin, C. S. Diercks, Y. B. Zhang, N. Kornienko, E. M. Nichols, Y. Zhao, A. R. Paris, D. Kim, P. Yang, O. M. Yaghi and C. J. Chang, *Science*, 2015, **349**, 1208-1213.
52. G. Lin, H. Ding, R. Chen, Z. Peng, B. Wang and C. Wang, *J*. *Am*. *Chem*. *Soc*., 2017, **139**, 8705-8709.

53. C. S. Diercks, S. Lin, N. Kornienko, E. A. Kapustin, E. M. Nichols, C. Zhu, Y. Zhao, C. J. Chang and O. M. Yaghi, *J. Am. Chem. Soc.*, 2018, **140**, 1116-1122.
54. R. Shen, W. Zhu, X. Yan, T. Li, Y. Liu, Y. Li, S. Dai and Z. G. Gu, *Chem. Commun.*, 2019, **55**, 822-825.
55. W. Lu, D. Yuan, D. Zhao, C. I. Schilling, O. Plietzsch, T. Muller, S. Bräse, J. Guenther, J. Blümel, R. Krishna, Z. Li and H.-C. Zhou, *Chem. Mater.*, 2010, **22**, 5964-5972.
56. J. Kim, B. Chen, T. M. Reineke, H. Li, M. Eddaoudi, D. B. Moler, M. O'Keeffe and O. M. Yaghi, *J. Am. Chem. Soc.*, 2001, **123**, 8239-8247.
57. F. J. Uribe-Romo, J. R. Hunt, H. Furukawa, C. Klöck, M. O'Keeffe and O. M. Yaghi, *J. Am. Chem. Soc.*, 2009, **131**, 4570-4571.
58. Z. Xiang, R. Mercado, J. M. Huck, H. Wang, Z. Guo, W. Wang, D. Cao, M. Haranczyk and B. Smit, *J. Am. Chem. Soc.*, 2015, **137**, 13301-13307.
59. B. Koszarna and D. T. Gryko, *J. Org. Chem.*, 2006, **71**, 3707-3717.
60. H. Doucet and J. C. Hierso, *Angew. Chem. Int. Ed.*, 2007, **46**, 834-871.
61. M. Gazvoda, M. Virant, B. Pinter and J. Košmrlj, *Nat. Commun.*, 2018, **9**, 4814-4823.
62. D. R. Lide, *CRC Handbook of Chemistry and Physics*, Taylor and Francis, 2005.
63. A. Laybourn, R. Dawson, R. Clowes, T. Hasell, A. I. Cooper, Y. Z. Khimyak and D. J. Adams, *Polym. Chem.*, 2014, **5**, 6325-6333.
64. S. Roy, A. Bandyopadhyay, M. Das, P. P. Ray, S. K. Pati and T. K. Maji, *J. Mater. Chem. A*, 2018, **6**, 5587-5591.
65. N. Keller, M. Calik, D. Sharapa, H. R. Soni, P. M. Zehetmaier, S. Rager, F. Auras, A. C. Jakowetz, A. Gorling, T. Clark and T. Bein, *J. Am. Chem. Soc.*, 2018, **140**, 16544-16552.
66. K. S. W. Sing, D. H. Everett, R. A. W. Haul, L. Moscou, R. A. Pierotti, J. Rouquérol and T. Siemieniewska, *Pure Appl. Chem.*, 1985, **57**, 603-619.
67. T. Zhao, C. Heering, I. Boldog, K. V. Domasevitch and C. Janiak, *CrystEngComm*, 2017, **19**, 776-780.
68. K. M. Patil, S. G. Telfer, S. C. Moratti, O. T. Qazvini and L. R. Hanton, *CrystEngComm*, 2017, **19**, 7236-7243.
69. M. J. Zaworotko, *Chem. Soc. Rev.*, 1994, **23**, 283-288.
70. V. A. Blatov, L. Carlucci, G. Ciani and D. M. Proserpio, *CrystEngComm*, 2004, **6**, 377-395.
71. L.-H. Xie and M. P. Suh, *Chem. Eur. J.*, 2011, **17**, 13653-13656.
72. S. Kumar, M. Y. Wani, C. T. Arranja, J. A. e Silva, B. Avula and A. J. F. N. Sobral, *J. Mater. Chem. A*, 2015, **3**, 19615-19637.

73. G. Lu, Y. Zhu, K. Xu, Y. Jin, Z. J. Ren, Z. Liu and W. Zhang, *Nanoscale*, 2015, **7**, 18271-18277.
74. J. Hynek, J. Zelenka, J. Rathousky, P. Kubat, T. Ruml, J. Demel and K. Lang, *ACS Appl. Mater. Interfaces*, 2018, **10**, 8527-8535.
75. E. D. Bloch, M. R. Hudson, J. A. Mason, S. Chavan, V. Crocellà, J. D. Howe, K. Lee, A. L. Dzubak, W. L. Queen, J. M. Zadrozny, S. J. Geier, L.-C. Lin, L. Gagliardi, B. Smit, J. B. Neaton, S. Bordiga, C. M. Brown and J. R. Long, *J. Am. Chem. Soc.*, 2014, **136**, 10752-10761.
76. J.-R. Li, Y. Ma, M. C. McCarthy, J. Sculley, J. Yu, H.-K. Jeong, P. B. Balbuena and H.-C. Zhou, *Coord. Chem. Rev.*, 2011, **255**, 1791-1823.
77. J. A. Mason, K. Sumida, Z. R. Herm, R. Krishna and J. R. Long, *Energy Environ. Sci.*, 2011, **4**, 3030-3040.
78. G. Ortiz, S. Brandès, Y. Rousselin and R. Guilard, *Chem. Eur. J.*, 2011, **17**, 6689-6695.
79. H. Feuchter, G. Ortiz, Y. Rousselin, A. Bessmertnykh-Lemeune and S. Brandès, *Cryst. Growth. Des.*, 2017, **17**, 3665-3676.
80. K. Sumida, D. L. Rogow, J. A. Mason, T. M. McDonald, E. D. Bloch, Z. R. Herm, T.-H. Bae and J. R. Long, *Chem. Rev.*, 2012, **112**, 724-781.
81. B. Li, Q. Sun, Y. Zhang, C. W. Abney, B. Aguila, W. Lin and S. Ma, *ACS Appl. Mater. Interfaces*, 2017, **9**, 12511-12517.
82. M. Xu, X. Han, T. Wang, S. Li and D. Hua, *J. Mater. Chem. A*, 2018, **6**, 13894-13900.
83. G. Frenking and N. Fröhlich, *Chem. Rev.*, 2000, **100**, 717-774.
84. M. Zhou, L. Andrews and C. W. Bauschlicher, *Chem. Rev.*, 2001, **101**, 1931-1962.
85. K. Nakamoto, in *Infrared and Raman Spectra of Inorganic and Coordination Compounds. Part B: Applications in Coordination, Organometallic, and Bioinorganic Chemistry*, John Wiley & Sons, 2009, pp. 132-152.
86. X. Wu, L. Zhao, D. Jiang, I. Fernandez, R. Berger, M. Zhou and G. Frenking, *Angew. Chem. Int. Ed.*, 2018, **57**, 3974-3980.
87. R. Guilard, C. P. Gros, F. Bolze, F. Jérôme, Z. Ou, J. Shao, J. Fischer, R. Weiss and K. M. Kadish, *Inorg. Chem.*, 2001, **40**, 4845-4855.
88. S. Zhu, Y. Liu, G. Wu, L. Fei, S. Zhang, Y. Hu, Z. Yan, Y. Wang, H. Gu and W. Chen, *Sens. Actuators B, Chem*, 2019, **285**, 49-55.